# High power nano-$LiMn_2O_4$ cathode materials with high-rate pulse discharge capability for lithium-ion batteries*

Chen Ying-Chao(陈颖超)†, Xie Kai(谢 凯), Pan Yi(盘 毅), Zheng Chun-Man(郑春满), and Wang Hua-Lin(王华林)

*Department of Material Engineering and Applied Chemistry, College of Aerospace and Materials Engineering, National University of Defense Technology, Changsha 410073, China*

(Received 3 March 2010; revised manuscript received 24 November 2010)

Nano-$LiMn_2O_4$ cathode materials with nano-sized particles are synthesized via a citric acid assisted sol–gel route. The structure, the morphology and the electrochemical properties of the nano-$LiMn_2O_4$ are investigated. Compared with the micro-sized $LiMn_2O_4$, the nano-$LiMn_2O_4$ possesses a high initial capacity (120 mAh/g) at a discharge rate of 0.2 C (29.6 mA/g). The nano-$LiMn_2O_4$ also has a good high-rate discharge capability, retaining 91% of its capacity at a discharge rate of 10 C and 73% at a discharge rate of 40 C. In particular, the nano-$LiMn_2O_4$ shows an excellent high-rate pulse discharge capability. The cut-off voltage at the end of 50-ms pulse discharge with a discharge rate of 80 C is above 3.40 V, and the voltage returns to over 4.10 V after the pulse discharge. These results show that the prepared nano-$LiMn_2O_4$ could be a potential cathode material for the power sources with the capability to deliver very high-rate pulse currents.

**Keywords:** lithium-ion batteries, lithium manganese oxide, high-rate, pulse discharge

**PACS:** 82.47.Aa, 82.45.Yz **DOI:** 10.1088/1674-1056/20/2/028201

## 1. Introduction

During the last decade, rechargeable lithium-ion batteries have been extensively investigated. They are widely used in portable electric devices, owing to their high energy densities.[1−3] However, until now the lithium-ion batteries are still incapable of delivering very high pulse currents as distinguished from the continuous discharge, which is required in some special applications, such as automatic meter readers, global positioning system (GPS) tracking devices, portable medical equipments, thermal imaging devices and laser devices.[4] The batteries still need to be improved. The high-power capabilities of the lithium-ion batteries are usually governed by the high-rate capabilities of the electrode materials. So it is important to investigate the cathode material used in the lithium-ion batteries.

In recent years, the synthesis of nano-structured electrode materials for the lithium-ion batteries has become an interesting research topic, because the reduced dimensions of the electrode materials enable the batteries to possess much higher power density.[5] The nano-sized spinel $LiMn_2O_4$ has attracted particular attention, owing to its excellent rate performance, high potential, low cost, low toxicity and high safety.[6−8] Several methods, including sol–gel method,[9] Pechini process,[10] combustion process,[11] explosive process,[12] chemical precipitation and hydrothermal methods, have been developed to obtain the nano-sized spinel $LiMn_2O_4$.

In this study, we present a citric acid assisted sol–gel method to synthesize the spinel $LiMn_2O_4$ with nano-sized particles. It exhibits an excellent high-rate capability, retaining 91% of its total capacity at a discharge rate of 10 C (1 C = 148 mA/g) and 73% of its total capacity at discharge rate of 40 C. We have paid special attention to the high-rate pulse discharge capability of the nano-$LiMn_2O_4$, which has rarely been investigated in previous studies.

## 2. Experiment

Two $LiMn_2O_4$ samples with different particle sizes were prepared for this study: the nano-$LiMn_2O_4$, hereafter referred to as nano-LMO, and the commercial $LiMn_2O_4$ with micro-meter size particles prepared

*Project supported by the National Natural Science Foundation for Postdoctoral Scientists of China (Grant No. 20090451554).
†Corresponding author. E-mail: cycdh2007@yahoo.cn
© 2011 Chinese Physical Society and IOP Publishing Ltd

by the solid-state reaction method, named micro-LMO.

The nano-LMO powder was synthesized by the sol–gel method, with citric acid serving as the chelating agent. 0.2-mol $LiNO_3$ (Alfa, 99%), 0.4-mol $Mn(NO_3)_2$ (Alfa, 50% in water solution) and 0.6-mol citric acid (Alfa, 99%) were dissolved into de-ionized water and mixed thoroughly. This solution was continuously stirred and gently heated to maintain complete homogeneity, while the solution pH was adjusted to 6.0 by adding ammonium hydroxide. Then the temperature of the solution was maintained at 80 °C until a transparent sol was obtained. Finally, the resultant sol was dried in the vacuum at 100 °C for 12 h to form a porous, foam-like solid. The foam-like precursor was pyrolyzed into fine powder in air at 400 °C for 5 h and then calcined in air at 750 °C for 5 h. After cooling, the nano-sized $LiMn_2O_4$ powder was obtained.

The crystal structure of the powder was identified with x-ray powder diffraction (XRD) analysis using a Japan-made diffractometer (D/Max-2500). The particle size and the morphology were investigated with a high-resolution transmission electron microscopy (HRTEM) (JEOL JEM-3010) and a field emission scanning electron microscopy (FESEM) (Hitachi S-4800). The surface areas of the powder were measured with the Brunauer–Emmett–Teller (BET) method through using a NOVA-1000 instrument and nitrogen gas.

The positive electrodes were typically made of 80 wt% active materials, 10 wt% acetylene black (as the conductive agent), and 10 wt% aqueous binder. The loading mass of $LiMn_2O_4$ in the prepared composite electrode was 3–4 mg/cm$^2$. The cells were assembled in an argon-filled glove box (MIKROUNA, China). Lithium metal was used as the counter electrode and the reference electrode. The 1-mol/L $LiPF_6$ in EC/DEC (1/1 by volume) was used as the electrolyte and Celgard 2400 was used as the separator.

Cyclic voltammogram (CV) was taken via a three-electrode system, in which the $LiMn_2O_4$ was used as the working electrode and the lithium metals were used as the counter electrode and the reference electrode. The scan was performed at a scan speed of 0.1 mV/s over a potential range of 3.2 V–4.5 V using an AUTOLAB PGSTAT30 electrochemical workstation. Charge/discharge studies were carried out on a two-electrode Swagelok test cell. The pulse discharge tests were performed on an AUTOLAB PGSTAT30 electrochemical workstation. The continuous discharge tests were performed on a multi-channel battery tester (LAND CT2001A) operating in galvanostatic mode. All the tests were performed at room temperature.

# 3. Results and discussion

## 3.1. Structure and morphology

The XRD patterns of nano-LMO and micro-LMO are shown in Fig. 1. The result indicates that two samples have identical crystal structures. All the diffraction peaks can be ascribed to originating from the cubic spinel structure with space group $Fd3m$, wherein the lithium ions occupy 8a sites, manganese ions 16d sites, and oxygen ions 32e sites. The diffraction pattern is in good agreement with the JCPDS standard (JCPDS 35-0782) and the results of others groups.[13–15] No other crystal phase or obvious impurity peaks were detected. The peaks of nano-LMO are relatively broad and weak due to the small grain sizes.

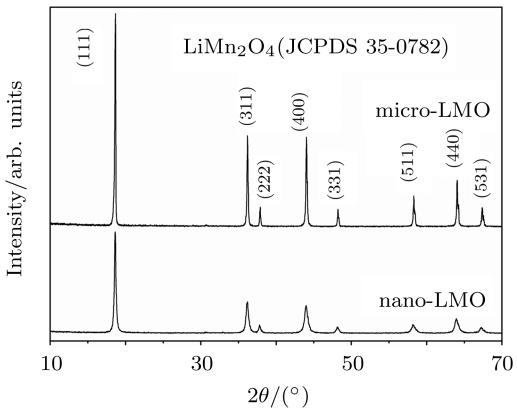



**Fig. 1.** XRD patterns of nano-LMO and micro-LMO.

Figure 2 shows the FESEM images and the HRTEM images of nano-LMO and micro-LMO. Aggregates are observed in the nano-LMO (Fig. 2(a)). These aggregates are composed of nano-sized particles (30 nm–80 nm) cemented together in the calcination process. Figure 2(b) shows a typical FESEM image of the commercial micro-LMO. It can be seen that the active mass contributes to nearly cubic morphology that is composed of particles with particle sizes in a range of 0.5 $\mu$m–3 $\mu$m. Figures 2(c) and 2(d) show the HRTEM images of nano-LMO. It can be seen that the average grain size of nano-LMO is about 50 nm. The selected area electron diffraction (SAED) pattern is shown in the inset of Fig. 2(c). The SAED pattern confirms the cubic structure and the $Fd3m$ space group of the $LiMn_2O_4$.

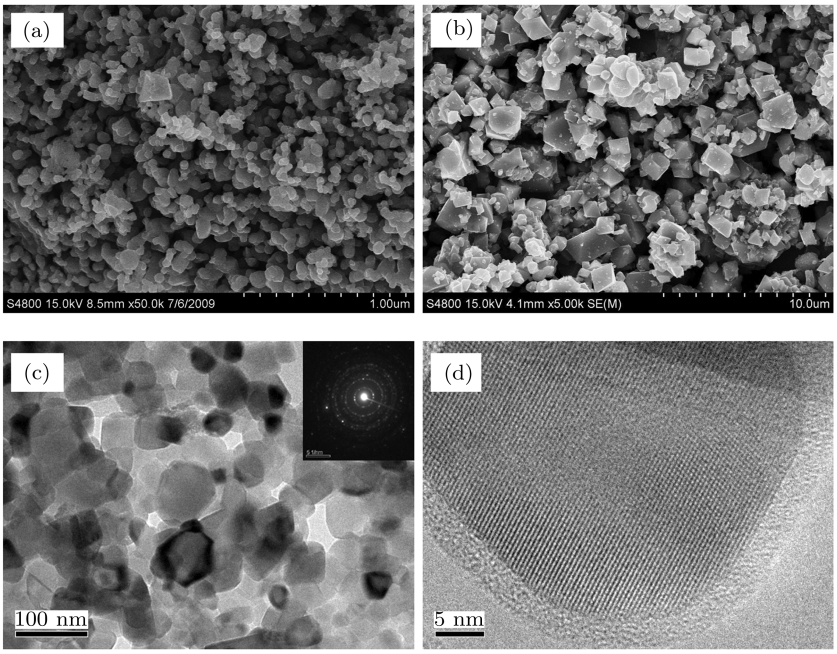



**Fig. 2.** (a) FESEM image of nano-LMO, (b) FESEM image of micro-LMO, (c) and (d) HRTEM images of nano-LMO.

The BET surface areas of nano-LMO and micro-LMO determined by $N_2$ desorption are 25.4 $m^2/g$ and 1.08 $m^2/g$, respectively. With the assumption that the shape of the particle is cubic, the particle size is calculated with the BET surface area by using the relationship, $A = 6/\rho l$, where $A$ is the BET surface area, $\rho$ is the mass density of spinel $LiMn_2O_4$ (4.281 $g/cm^3$), and $l$ is the particle size. The calculated particles sizes are 55 nm for the nano-LMO and 1.3 $\mu$m for the micro-LMO.

## 3.2. Electrochemical properties

Figure 3 shows the 2nd cycle normal CV scans in the potential window 3.2 V–4.5 V at a scan speed of 0.1 mV/s. The CV curves by both cells show two pairs of clearly separated oxidation/reduction peaks. The pair of peaks correspond to a two-step reversible intercalation reaction, in which lithium ions come from two different tetragonal 8a sites of the spinel $Li_xMn_2O_4$ ($x < 1$) at each step. The results are consistent with those reported in Refs. [16]–[18]. In comparison with the current peaks of the micro-LMO, the current peaks of nano-LMO are narrow and high and the separation of redox peak potentials ($\Delta\varphi_p$) is small. Narrower current peaks and smaller $\Delta\varphi_p$ indicate that the nano-LMO has higher electrochemical activity and lower overpotential.

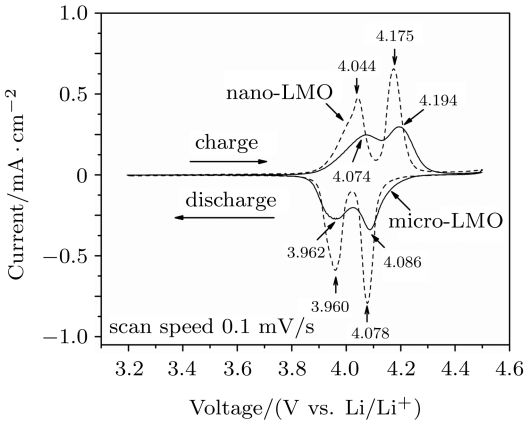



**Fig. 3.** CV curves of nano-LMO and micro-LMO at the 2nd cycle in the potential window 3.2–4.5 V (vs. $Li/Li^+$), where solid line is for micro-LMO, and dot line for nano-LMO.

Figure 4 shows the charge/discharge curves of nano-LMO and micro-LMO. Both samples exhibit two plateaus (around 3.95 V and 4.05 V respectively) on the discharge curves. This again is due to the two-step reduction/oxidation process, which is a characteristic of the spinel $LiMn_2O_4$. Figure 4 shows that the initial discharge capacities of nano-LMO and micro-LMO are 120 mAh/g and 112 mAh/g respectively at a discharge rate of 0.2 C (29.6 mA/g). In comparison with the nano-LMO, the micro-LMO has relatively low initial discharge capacity. The difference in initial charge/discharge capacity between the two

samples results from the difference among the particle sizes of $LiMn_2O_4$ powder. When the particle size is reduced, the overall surface area is increased. The BET surface area of nano-LMO (25.4 $m^2/g$) is much higher than that of micro-LMO (1.08 $m^2/g$). With larger surface area, the cathode composed of smaller particles can provide more lithium ions for diffusion, and so the specific capacity is increased.

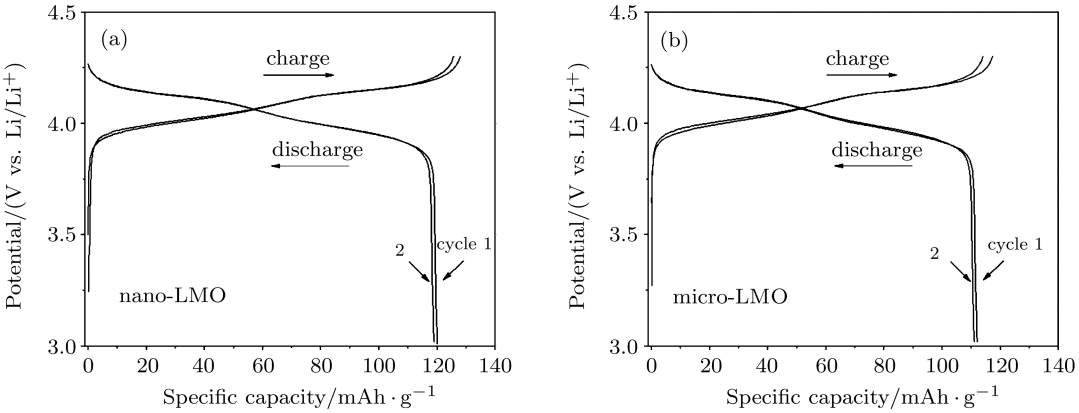



**Fig. 4.** Charge/discharge curves of nano-LMO and micro-LMO, between 3.0 V and 4.3 V at a discharge rate of 0.2 C (29.6 mA/g) for the first two cycles.

The rate capabilities of nano-LMO and micro-LMO are presented in Fig. 5. The rate capability is expressed as a ratio of the capacity at a given discharge rate to that obtained at the discharge rate of 0.2 C. The rate performance of nano-LMO is excellent, 91% of its total capacity is retained at a discharge rate of 10 C and 73% of its total capacity is retained at a discharge rate of 40 C. The discharge curves of nano-LMO and micro-LMO for different discharge rates (C-rates) are shown in Figs. 5(b) and 5(c). The poor electrochemical performance of micro-LMO at high current density is caused by the low surface area and the large particle size, which has been shown in the BET measurements and the FESEM investigations (Fig. 2(b)). Furthermore, the larger particle size of micro-LMO has barrier effect for $Li^+$ de-intercalation/intercalation. The lower BET surface and the larger particle size both lead to higher electrochemical polarization in the charge/discharge processes, resulting in a lower discharge capacity and a lower discharge plateau. Although in general the discharge plateau gradually shifts towards lower voltage and the discharge capacity decreases with C-rate increasing, these changes in nano-LMO are much smaller than those in previous reports.[15,19,20]

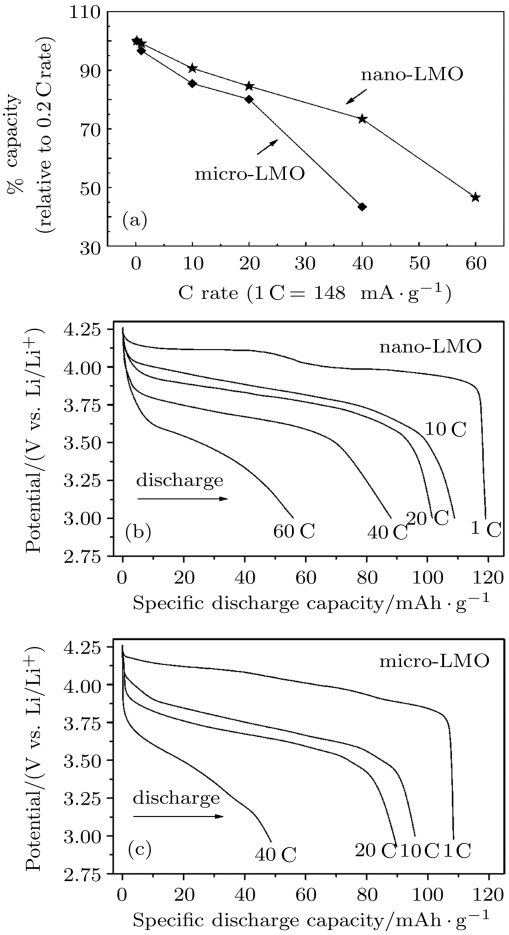



**Fig. 5.** (a) Rate performances of nano-LMO and micro-LMO. (b) and (c) Discharge curves of nano-LMO and micro-LMO at different C-rates. The cell is charged at a rate of 0.5 C and discharged at different C-rates, 1 C corresponds to 148 mA/g discharge specific capacity.

The high-rate pulse discharge curves of nano-LMO and micro-LMO are shown in Fig. 6. The cell is charged to 4.3 V at a rate of 0.5 C (74 mA/g) and then discharged for 50 ms at different pulse discharge rates (20 C–80 C). The discharge voltages for both samples decrease significantly with C-rate increasing. The potential drops off more significantly with the increase of discharge rate. This is caused by the resistance of the electrolyte at high discharge rate, while the large polarization results from the slow lithium diffusion in the active material. In comparison with the micro-LMO, the nano-LMO exhibits better high-rate pulse discharge performance: higher discharge voltage and higher cut-off voltage (Fig. 7). The excellent high-rate pulse discharge performance can be attributed to the higher BET surface area and the smaller particle size. The decrease in particle size leads to a significant increase in $Li^+$ de-intercalation/intercalation rate, because the distances for $Li^+$ and electron to travel within the particles are shortened. The decrease in particle size also implies a larger surface area, which permits a larger contact area with the electrolyte and a higher $Li^+$ flux across the interface.[21] As a result, the nano-LMO with larger BET surface area and nano-sized particles has lower electrochemical polarization in the charge/discharge processes, which leads to a higher discharge voltage plateau and a higher cut-off voltage.

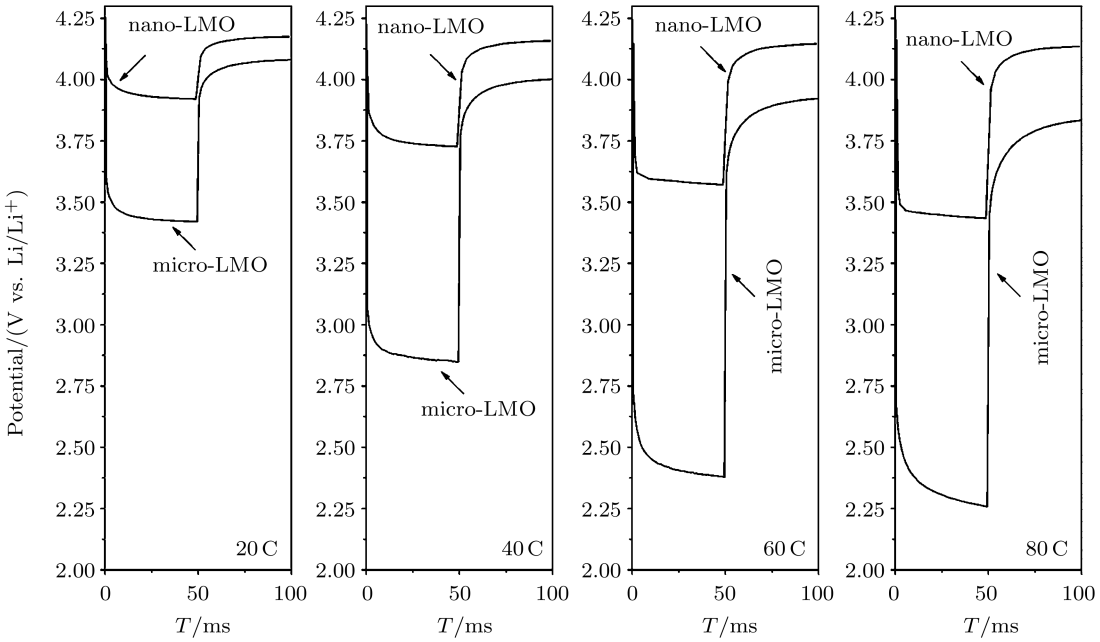



**Fig. 6.** The 50-ms pulse discharge curves of nano-LMO and micro-LMO at various discharge rates.

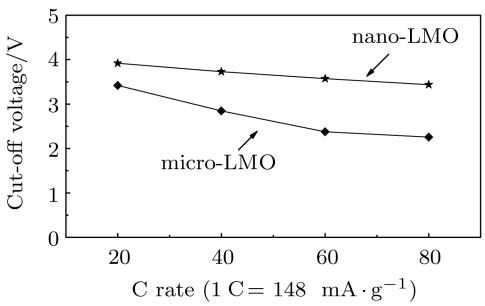



**Fig. 7.** Cut-off voltages of nano-LMO and micro-LMO at various discharge rates for 50-ms pulse discharge.

The variations of discharge capacity with cycle number, for up to 300 cycles, are shown in Fig. 8. The discharge capacity of nano-LMO at a discharge rate of 1 C, which is 118 mAh/g for the first cycle, decreases significantly on subsequent cycles, retaining a capacity of 87 mAh/g after 300 cycles. Although the initial capacity of micro-LMO was lower, the micro-LMO exhibited a better cycle performance, retaining 89 mAh/g at the end of 300 cycles. The coulombic efficiencies (calculated by discharge capacity/charge capacity) of nano-LMO and micro-LMO are shown in Fig. 8. In comparison with the micro-LMO, the nano-LMO has a low coulombic efficiency. The lower coulombic efficiency implies that more side reactions take place in the charge/discharge processes, which may be caused by the higher surface area of the nano-sized particles, resulting in a poorer cycle-ability

for the nano-LMO. Higher electrolyte/electrode contact area leads to more significant side reactions and so it is more difficult to maintain the interparticle contacts.[21]

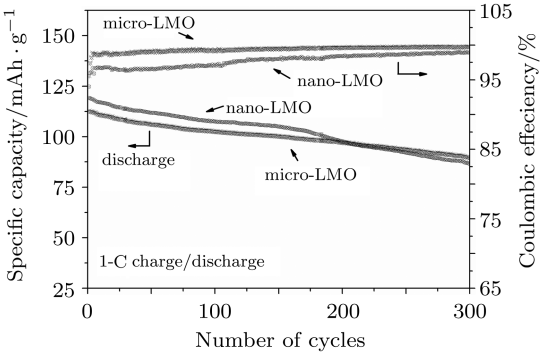



**Fig. 8.** Cycling performances of nano-LMO and micro-LMO at discharge rate of 1 C (148 mA/g).

# 4. Conclusions

The nano-LMO with nano-sized particles has been synthesized via citric acid assisted sol–gel route. In comparison with the micro-sized micro-LMO, the nano-LMO possesses a higher initial capacity (120 mAh/g) at a discharge rate of 0.2 C (29.6 mA/g). It also exhibits a good high-rate discharge capability, retaining 91% of its total capacity at a discharge rate of 10 C and 73% of its total capacity at a discharge rate of 40 C. In particular, the nano-LMO shows an excellent high-rate pulse discharge capability. The cut-off voltage at the end of 50-ms pulse discharge at very high discharge rate (80 C) is above 3.40 V, and the voltage returns to 4.10 V after the pulse discharge. These results show that the prepared nano-LMO is a potential cathode material for the power sources with the capability to deliver very high-rate pulse currents.

# References


[1] Tarascon J M and Armand M 2001 *Nature* **414** 359

[2] Shi S L, Liu Y G, Zhang J Y and Wang T H 2009 *Chin. Phys.* B **18** 4564

[3] Hou X H, Hu S J, Li W S, Ru Q, Yu H W and Huang Z W 2008 *Chin. Phys.* B **17** 3422

[4] Menachem C and Yamin H 2004 *J. Power Sources* **136** 268

[5] Jiang C H, Hosono E and Zhou H S 2006 *Nano Today* **1** 28

[6] Tarascon J M, Coowar F, Amatuci G, Shokoohi F K and Guyomard D G 1995 *J. Power Sources* **54** 103

[7] Manev V, Banov B, Momchilov A and Nassalevska A 1995 *J. Power Sources* **57** 99

[8] Hu G J and Ouyang C Y 2010 *Acta Phys. Sin.* **59** 5863 (in Chinese)

[9] Liu H, Wu Y P, Rahm E, Holze R and Wu H Q 2004 *J. Solid State Electron.* **8** 450

[10] Wu S H and Chen H L 2003 *J. Power Sources* **119–121** 134

[11] Zhang Y L, Shin H C, Dong J and Liu M L 2004 *Solid State Ionics* **171** 25

[12] Xie X H, Li X J, Zhao Z, Wu H B, Qu Y D and Huang W Y 2006 *Powder Technology* **169** 143

[13] Wang X, Chen X Y, Gao L S, Zheng H G, Ji M R, Shen T and Zhang Z D 2003 *J. Cryst. Growth* **256** 123

[14] Gadjov H, Gorova M, Kotzeva V, Avdeev G, Uzunova S and Kovacheva D 2004 *J. Power Sources* **134** 110

[15] Ye S H, Lü J Y, Gao X P, Wu F and Song D Y 2004 *Electrochimica Acta* **49** 1623

[16] Rougier A, Striebel K A, Wen S J and Cairns E J 1998 *J. Electrochem. Soc.* **145** 1975

[17] Wu H M, Tu J P, Yuan Y F, Li Y, Zhang W K and Huang H 2005 *Physica* B **369** 221

[18] Thirunakaran R, Kim K T, Kang Y M, Seo C Y and Jai Y L 2004 *J. Power Sources* **137** 100

[19] Park S H, Myung S T, Oh S W, Yoon C S and Sun Y K 2006 *Electrochimica Acta* **51** 4089

[20] Zhang Y L, Shin H C, Dong J and Liu M L 2004 *Solid State Ionics* **171** 25

[21] Bruce P G, Scrosati B and Tarascon J M 2008 *Angew. Chem. Int. Ed.* **47** 2930